

Epineuston vortex recapture enhances thrust in tiny water skaters

Pankaj Rohilla^{*a}, Johnathan N. O’Neil^{1a}, Chandan Bose^b, Victor M. Ortega-Jimenez^c, Daehyun Choi^a, and Saad Bhamla^{2a}

^a

School of Chemical and Biomolecular Engineering, Georgia Institute of Technology, Atlanta, GA, USA ^b*Aerospace Engineering, School of Metallurgy and Materials, University of Birmingham, Birmingham, UK* ^c*School of Biology and Ecology, University of Maine, ME, USA*

Vortex recapture underpins the exceptional mobility of nature’s finest fliers and swimmers. Utilized by agile fruit flies and efficient jellyfish, this phenomenon is well-documented in bulk fluids. Despite extensive studies on the neuston—a vital fluidic interface where diverse life forms interact between air and water—neuston vortical hydrodynamics remain unexplored. We investigate epineuston (on water) vortical hydrodynamics in *Microvelia americana*, one of the smallest and fastest water striders, skating at 50 BL/s (15 cm/s). Their middle legs shed counter-rotating vortices, re-energized by hind legs, demonstrating epineuston vortex recapture. High-speed imaging, particle imaging velocimetry, physical models, and CFD simulations show re-energization increases thrust by creating positive pressure at the hind tarsi, acting as a virtual wall. This vortex capture is facilitated by the tripod gait, leg morphology, and precise spatio-temporal placement of the hind tarsi during the power stroke. Our study extends vortex recapture principles from bulk fluids to the neuston, offering insights into efficient epineuston locomotion, where surface tension and capillary waves challenge movement. Understanding epineuston vortex hydrodynamics can guide the development of energy-efficient microrobots to explore the planet’s neuston niches, critical frontlines of climate change and pollution.

¹ Equal contribution

² Corresponding author- saadb@chbe.gatech.edu

1 The unseen ballet of vortical forces orchestrates 2 nature's niche ($\mathbf{u}_B \sim 50$ BL/s, Figure 2.d). Part of the 29
most efficient swimmers and fliers [1–7]. 3 These infraorder Gerromorpha, they are found in creeks 30
interactions, fundamental to minimizing en- 4 ergy expenditure and maximizing thrust, allow organisms 5 to utilize energy from their own or others' 6 wakes [1,2,8–10]. Unlike most water striders that 31
use elongated middle legs for rowing, *Microvelia* 32
10. Jellyfish boost thrust by capturing vortices during 7 relaxation, creating high-pressure 33
8 zones [5,11]. Fruit flies capture leading-edge vortices 9 kinematics enable them to recapture vortices shed 34
during the fling motion, minimizing the energy required to 10 from their middle legs, allowing them to speedily 35
generate new vortices [12,13]. Fish exhibit 11 such efficient wake capture that even dead fish can 12 swim 36
upstream by resonating with oncoming K'arm'an 13 street 37
vortices [14,15]. 38
14 While these examples occur in bulk fluids, the 15 neuston 39
interface — a vital ecological niche — teems 16 with life. From high-speed imaging, particle imaging velocimetry, 40
zooplankton, insects, and spiders to 17 birds, reptiles, and 41
plants, countless organisms 18 interact at this boundary in the epineuston vortex interactions during the water 42
marine and freshwater 19 ecosystems [16–27]. Despite the skating behavior of *Microvelia*. 43
challenges of bal- 44
20 ancing surface tension, drag, buoyancy, and capillary 45
waves, no documented examples of vortex re-capture at this 21
interface exist. Driven by curiosity 22 about neuston vortical 46
interactions, we reveal a vor-23 tex re-energization 47
mechanism in *Microvelia americana* (Hemiptera, Veliidae). 48
24 These millimeter-sized water walkers are 25 epineustonic, 49
living on the water surface and 26 are one of the smallest and 50
fastest on this ecological 27 51
28 52
29 53
30 54
31 55
32 56
33 57
34 58
35 59
36 60
37 61
38 62
39 63
40 64
41 65
42 66
43 67
44 68
45 69
46 70
47 71
48 72
49 73
50 74
51 75
52 76
53 77
54 78
55 79
56 80

RESULTS

Skating on water. *Microvelia* possess dense hair coverage on their bodies and legs (Figure 1.a) [38]. SEM analysis reveals a tarsal hair density of $\sim 15,000$ hairs/mm² ($n = 3$), comparable to *Velia caprai* and *Gerridae*. [16, 39, 40]. This dense coverage enables *Microvelia* to maintain a Cassie-Baxter state [41], limiting water infiltration and maintaining superhydrophobicity leading to dimples at air-water surface contact points (Figure 1.b). The low Weber number, $We = \rho v^2 l / \sigma \ll 1$ (see Table S1) indicates that

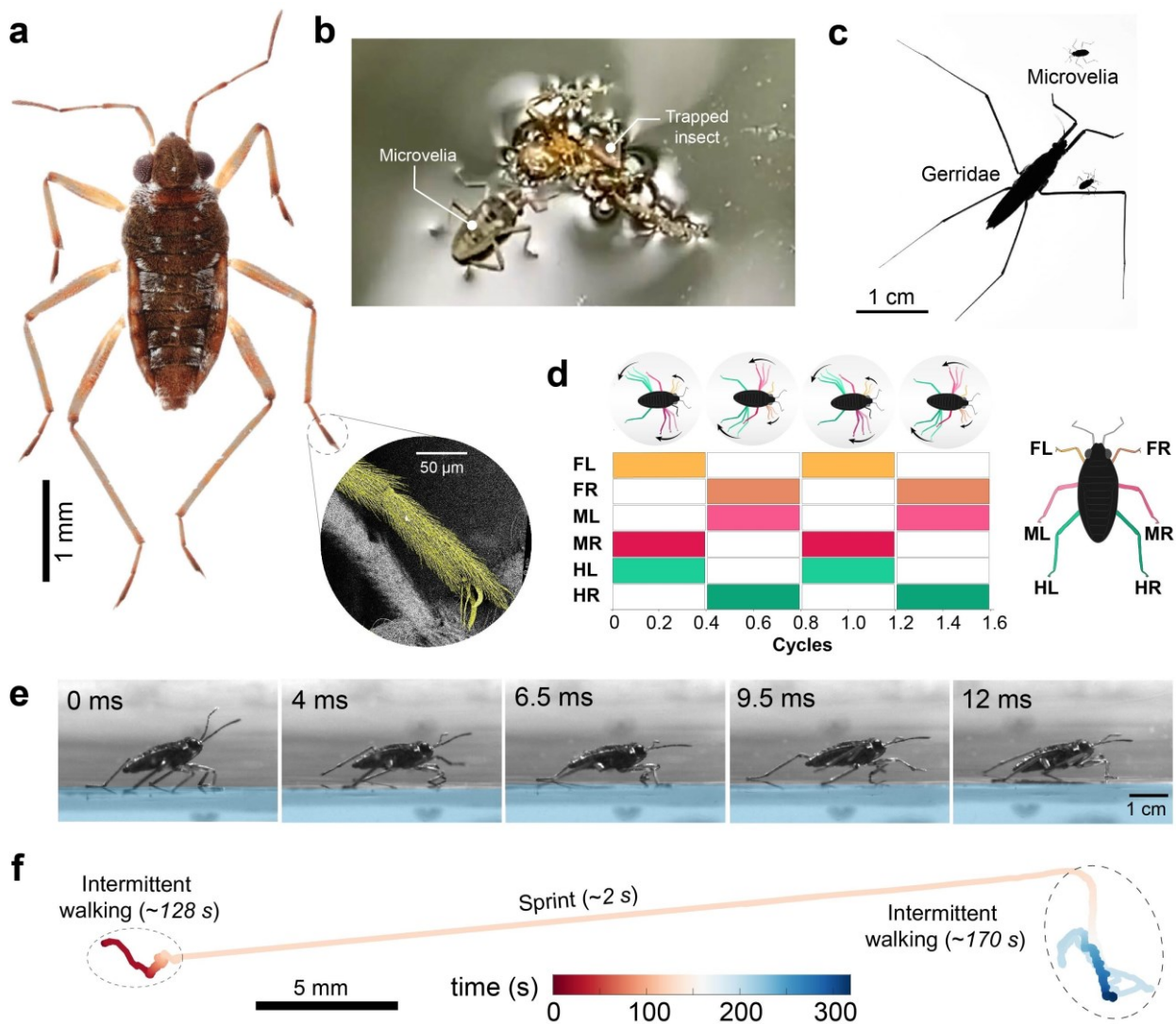


Figure 1: Behaviour and morphology of epineustonic *Microvelia americana* **(a)** Dorsal view of *Microvelia americana* with a 1 mm scale bar. Inset shows a SEM image of the middle leg tarsus (*pseudo-colored*). **(b)** *Microvelia Sp.* feeding on a trapped insect in a creek (Brunei), with legs deforming the water surface, forming dimples. **(c)** Size comparison showing *M. americana*'s small body size relative to commonly found water striders, *Gerridae*. **(d)** Alternating tripod gait plot for *M. americana* locomoting on water surface, showing the gait cycle of each leg performing power (color filled boxes) and recovery strokes (empty boxes). **(e)** Snapshots showing the side view of *M. americana* walking on water. **(f)** Dynamics of *M. americana* on water, indicating short skating escape-sprints (~2 s) and intermittent walking behavior over a time span 5 minutes.

57 surface tension forces dominate over inertial forces 58 in (SI Video 1).
 59 their interfacial locomotion, similar to other water striders 60 To understand their epineustonic locomotion be-
 61 like Gerridae [24].

62 Unlike water striders such as *Gerridae* that use a 63 primarily engage in intermittent walking, spending
 64 gait typical of terrestrial insects. In this gait, at least 65 99.6% of the time in this mode. However, they occa-
 66 three legs – the front leg (FL), the contralateral mid- 67 sionally sprint as an escape response, skating a dis-
 68 leg (ML), and the ipsilateral hind leg (HL) – per- 69 tance of ~ 30 mm in ~ 2 seconds (Figure 1.e). The
 70 form a power stroke on water (Figure 1.d,e), while 71 the temporal trajectory of the middle and hind legs shows
 72 other legs recover in air or sometimes on water 73 overlapping paths during this skating mode, indicat-
 74 75 76

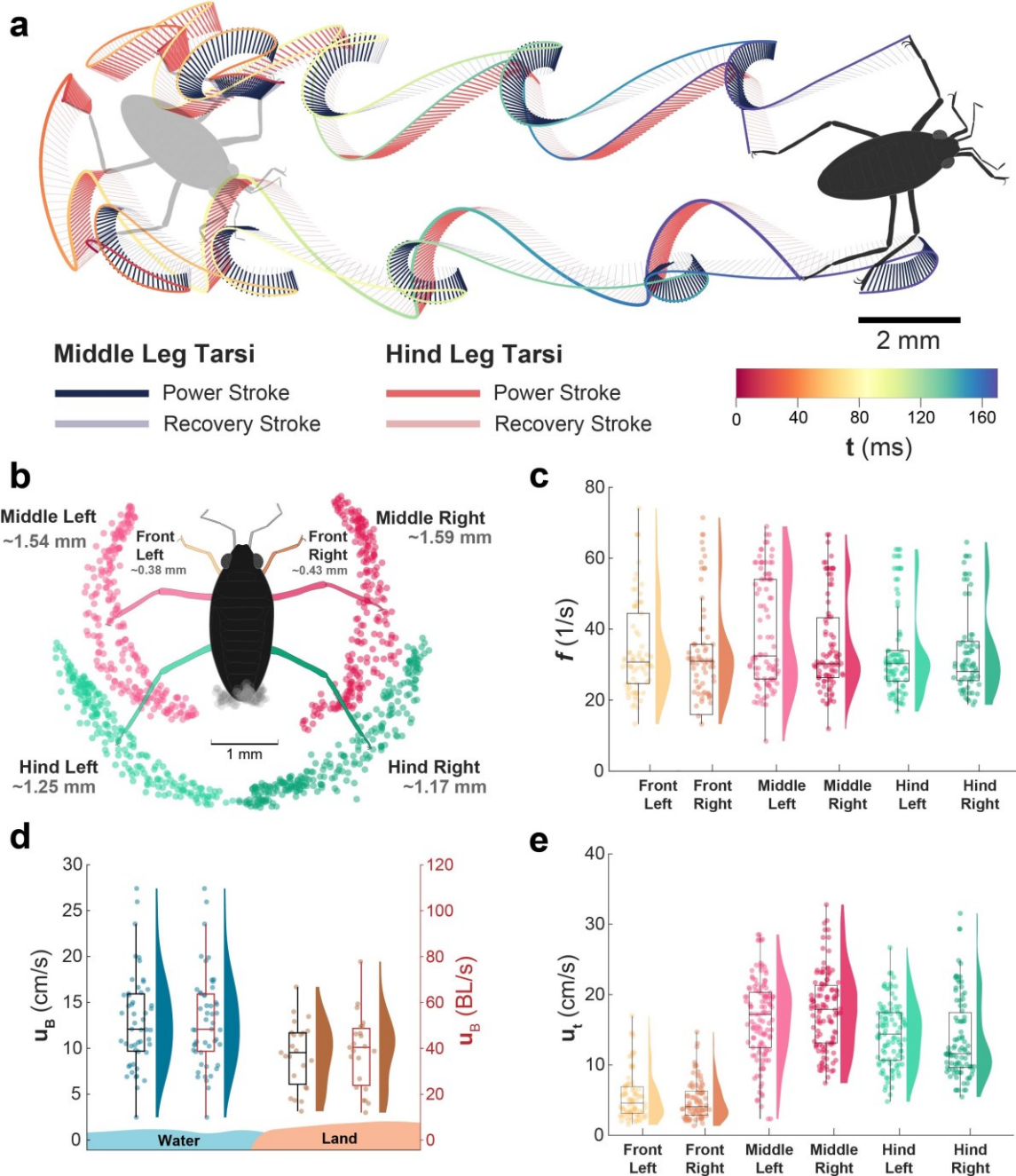


Figure 2: Epineustonic kinematics of *Microvelia*. **(a)** Tarsal trajectories of middle and hind legs of *Microvelia*. The solid lines represent the power strokes, while the faded blue and red lines show the recovery strokes. The trajectories illustrate the time spent by the tarsi during movement. **(b)** Stroke amplitudes of the middle and hind legs ($n = 15$), illustrated with their tarsal tip trajectories relative to the motion of their respective shoulder joints. The middle legs exhibit larger stroke amplitudes ($\lambda_{ML} \sim 1.54 \pm 0.43$ mm and $\lambda_{MR} \sim 1.59 \pm 0.74$ mm) compared to the hind legs ($\lambda_{HL} \sim 1.25 \pm 0.46$ mm and $\lambda_{HR} \sim 1.17 \pm 0.47$ mm). **(c)** Stroke frequency ($N = 3$, $n = 15$) of the middle and hind tarsi, showing an average stroke frequency of $f \sim 30$ strokes/s. **(d)** Body speed of *Microvelia* on water and land (styrofoam) in cm/s (left Y axis) and BL/s (body lengths per second, right Y axis). The average maximum body speed on water is ~ 15 cm/s (~ 50 BL/s), compared to ~ 10 cm/s (~ 40 BL/s) on land. **(e)** Peak tarsi speeds of *Microvelia* on water. The middle legs achieve higher peak linear speeds during power strokes (~ 17 cm/s) compared to the hind legs (~ 14 cm/s). This indicates that the middle legs act as the main hydrodynamic thrust propulsors, with higher acceleration (~ 2500 cm²/s) compared to the hind legs (~ 2000 cm²/s).

tex annihilation (Figure 3.e). We compare the normalized peak circulation before and after their hind tarsal interaction ($\Gamma = \tilde{\Gamma}_2/\Gamma_1$) with normalized body speed ($\tilde{\mathbf{u}} = \mathbf{u}_B/\mathbf{u}_t$) and the time interval (Δt) between strokes (Figure 3.d). Vortical re-energization primarily occurs when the hind tarsi strike between the middle tarsi vortices with shorter Δt (typically < 6 ms), during initial acceleration phase of the skating sprint (Figure 3.f). At higher body speeds, longer Δt , or due to body turning or rocking, the hind tarsi miss the vortices resulting in no interaction. When the hind legs skate across the pair of vortices rather than slaloming between them, the interactions tend to weaken the vortices, leading to vortex annihilation (Figure 3.d). Collectively, this reinforces that both the hind tarsi's entry position relative to the middle tarsi (angle-of-attack) and the inter-stroke interval play critical roles in determining the outcome of these interactions.

Epineuston vortical recapture increases thrust in *Microvelia*. Reconstructed pressure fields from PIV-measured velocity fields reveal insights into vortical interactions with the hind tarsi of *Microvelia* (Figure 4.a). During vortex re-energization, a local pressure gradient forms from upstream to downstream of the hind tarsi, generating the highest relative pressure ($\Delta p \sim 5$ Pa). In contrast, vortex annihilation results in lower relative pressure ($\Delta p \sim 2$ Pa, Figure S3), with cases of no interaction showing similarly low pressure.

We calculate the total impulse by integrating the relative pressure over time, $\mathbf{I} = R_T \Delta p A dt$, where T is the duration of the power stroke and A is the planar area containing the tarsi and its wake (Figure S3).

Normalizing the impulse, $\tilde{\mathbf{I}} = R_T \Delta p dt / (\rho \tilde{\mathbf{u}}_{t,n}^2 A)$, isolates the impact of hind tarsal interaction from tarsal speed. Excluding the impulse from the middle tarsi yields the relative impulse, $\tilde{\mathbf{I}}_r = \tilde{\mathbf{I}} / \tilde{\mathbf{I}}_{middle}$.

Our results show that vortex re-energization produces a normalized impulse ($\tilde{\mathbf{I}}_r \sim 1.08$), 34% higher than vortex annihilation (~ 0.81) and 15% higher than no interaction (~ 0.94) (Figure 4.b). This increased impulse results from enhanced fluid entrainment during re-energization, which raises pressure in the tarsal plane. When hind tarsi step into the center of the vortex pair, they entrain more fluid mass due to the converging flow driven by the vortical motion [44], leading to increased pressure and greater

77 ing interfacial vortical interactions (Figure 2.a). thrust. 179

78 During the skating mode, the middle legs of *Microvelia* crovelia 180 act as the main hydrodynamic thrust propulsors [32], re-energization 181 illustrates *Microvelia*'s ability to har- 182 33]. These legs exhibit a stroke amplitude 23% larger than the hind legs, while maintaining the same stroke call 'Epineuston Vortex Recapture'. Typically, wakes 183 frequency (Figure 2.b,c). This larger amplitude allows 184 signifies lost energy to the environment. By step- 185 for greater displacement with each stroke, enhancing thrust. The mid- 186 dle legs also achieve higher peak linear speeds during power strokes, 21% faster than the hind legs (Figure 187 2.e). This increased speed, coupled with greater acceleration—about 25% higher than that of the hind legs— 188 indicates their dominant role as forceful thrust generators [33].

91 **Epineuston hydrodynamic interactions.** During the power stroke, the middle leg tarsi shed pairs of counter- 92 rotating vortices (Figure 3.a, stage I). 93 These vortices travel downstream, interacting with the hind tarsi, which 94 enter the water at various spatio-temporal locations. The front tarsi generate weak vortices that dissipate 95 without interacting with other tarsi (SI video II). 96

99 The exact location and timing of the incident hind tarsi relative to the vortices dictate the outcome of these 100 interactions. Favourable interactions result in vortex re-energization, increasing the vortices' strength (Figure 3.a, Stage II and III). Body rocking and 101 turning can misalign these interactions, altering the hind legs' angle of attack and leading to vortex annihilation or no interaction (Figure 3.b). Additionally, if *Microvelia* moves at high speed, its body can pass over the middle 102 leg vortices before the hind legs can interact with them, emphasizing the importance of timing (Figure 3.f).

111 We measure the circulation of vortex pairs generated by the middle tarsi during re-energization until they 112 dissipate after hind tarsi interaction. Circulation, $\Gamma = \int \mathbf{R}_s \omega \cdot d\mathbf{S}$, where ω is the vorticity and S is the bounded 113 area, measures the vortices' strength. As the middle leg initiates the power stroke (Figure 3.c, point 1), the 114 vortices' circulation increases, peaking at $\Gamma = 2 \text{ cm}^2/\text{s}$ ($t = 71 \text{ ms}$), corresponding to the maximum tarsal speed 115 (22 cm/s, $t = 70 \text{ ms}$). The middle leg then decelerates, reducing Γ as the vortices dissipate (point 3). The hind 116 tarsi then enters the wake, re-energizing the vortices to enhance the circulation to a second, lower peak of $\Gamma = 1.6 \text{ cm}^2/\text{s}$ ($t = 88.5 \text{ ms}$) due to a lower hind-tarsal speed of 17 cm/s (Figure 3.c, point 4). This cycle ends with the hind 117 tarsi completing their power stroke and dissipating the vortices (SI video II, Figure S2).

128 Across 52 instances in 6 specimens, we observe that 60% of the interactions result in re-energization, 27% show no interaction, and the remainder lead to vor-

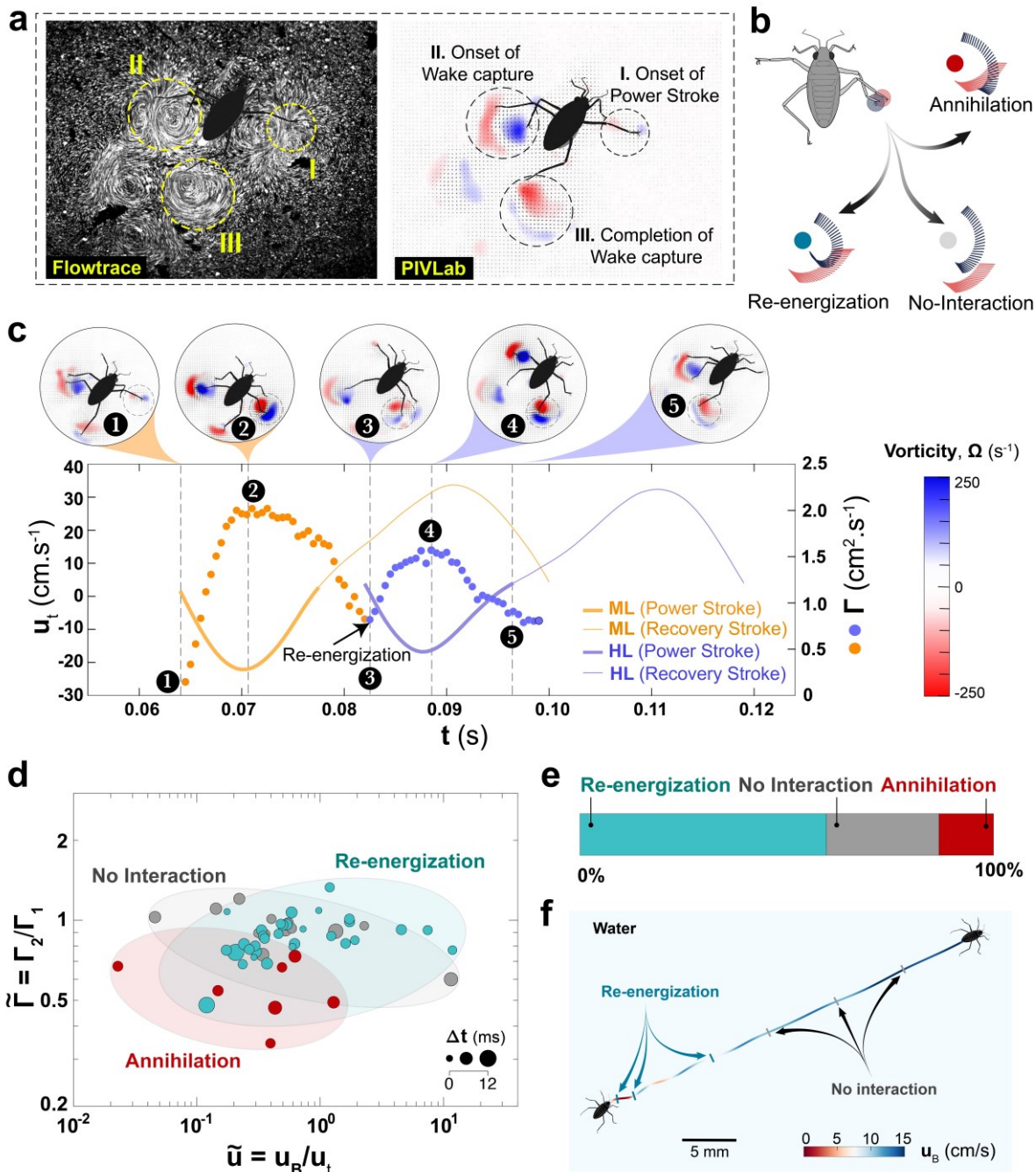


Figure 3: Hydrodynamic interactions in *Microvelia*'s epineustonic locomotion. **(a)** Stages of vortical shedding from the power strokes of the middle tarsus and their subsequent interactions with the hind tarsus. LHS: Flowfield streamlines visualization in Flowtrace [42] and RHS: vorticity field generated in PIVlab [43]. Stage I Vortices generated during the onset of the power stroke of the middle right tarsus, (II) Hind legs stepping into the vortices shed from the middle left tarsus, (III) re-energized vortices from the hind right tarsus; LHS shows the vorticity field corresponding to the frame on the right. **(b)** Illustrations represent the three different outcomes of vortical interactions based on the trajectory of the hind and middle tarsi. **(c)** Representative tarsal velocity profiles of the middle-right and hind-right tarsi of *Microvelia* walking on water and the corresponding circulation (filled circles) of the vortices for the case of vortex re-energization. **(d)** Effect of normalized body speed (relative to hind tarsi speed) on the circulation ratio of vortices originating from the middle legs pre- and post-

interactions with the hind tarsi. **(e)** Percentage outcomes of the vortical interactions of the hind tarsi with vortices shed from the middle tarsi, and **(f)** Different vortical interactions within a single run on water in *Microvelia*.

ond plate fails to interact effectively, leading to vortex annihilation with lower flow velocities and thrust due to the absence of effective wake capture.

To reinforce our findings, we present the temporal evolution of the coefficient of thrust (C_T) for the second plate, showing vortical re-energization, compared to no interaction (Figure 4.f). The C_T , defined as $2T/(\rho_r \mathbf{u}_r^2 A)$, where T is the thrust force, ρ_r is the fluid density, \mathbf{u}_r is the relative linear velocity, and A is the plate's projected area, illustrates the influence of interaction on vorticity fields at different times.

For $\Delta t = 0.2$ s, C_T peaks at $t = 1.2$ s as vortex dipoles from both plates interact, augmenting circulation. As the plates separate, C_T decreases, showing reduced wake interaction. Thrust enhancement via wake capture correlates with changes in fluid impulse, influenced by circulation and vortex core velocities. This unsteady flow situation is consistent with pressure data from *Microvelia* and the physical model (Figure 4.a,b), where optimal stroke timing increases entrainment and thrust, demonstrating enhanced thrust through vortex re-energization.

Conclusions and Outlook

Our findings illuminate vortical interactions within the neuston, the dynamic water-air boundary that supports diverse life forms. *Microvelia*, among one of the smallest and fastest epineustonic animals, create nearly 2D vortices due to their minute size and weight, forming shallow dimples on the water surface [45,46]. Their alternating tripod gait, inherited from terrestrial ancestors, enables versatile movement across water, land, and duckweed [17,32,47].

Although less energy-efficient than rowing gait, the alternative tripod gait excels in amphibious locomotion, providing *Microvelia* with a strategic advantage in foraging and evading predators [16,24,46]. This gait and leg proportions facilitate epineustron vortex recapture combination, where hind leg tarsi boost the circulation and fluid entrainment of vortices shed by middle legs. This re-energization creates a positive pressure at the hind tarsi, acting as a virtual wall that augments thrust [46]. In other genera such as *Mesovelia*, longer middle legs prevent effective vortex recapture, underscoring the critical role of leg size in this mechanism (Figure S7).

Epineuston vortex interactions hinge on the spatial location, angle of attack, and trajectory of hind leg tarsi, determining whether vortices are re-energized, annihilated, or minimally interacted with. Our

185 ping into vortices generated by its middle legs during 186 previous strokes, *Microvelia* harnesses this energy to 187 increase thrust production by the hind legs. This 188 movement, enables *Microvelia* to effectively generate 189 thrust at the air-water interface.

288
289
290

191 **Physical models validate inter-stroke interval 192 in epineustonic vortical interactions.** To evaluate the 193 effect of inter-stroke intervals (Δt) on vortical interactions, we use a physical model. The model 195 simulates *Microvelia*'s middle and hind tarsi power 196 strokes on water, varying Δt to alter the hind tarsi's 197 angle of attack to the vortices shed by the middle 198 legs. The Reynolds number of the model (~ 18) is 199 within the range of *Microvelia* ($Re \sim 2 - 21$, see Table 200 S1). The first arm generates a counter-rotating 201 vortex dipole, which the second arm interacts with, 202 depending on Δt (Figure 4.c).

203 For large $\Delta t = -116$ ms, the first arm's vortices 204 dissipate before the second arm's entry, resulting in 205 no interaction (SI Video III, Figure S4). Reducing the 206 interval allows for re-energization, with the second 207 arm's vortices showing higher normalized circulation 208 ($\tilde{\Gamma} > 1$) (Figure 4.d). However, at very short intervals 209 ($-10 < \Delta t < 10$ ms), capillary waves generated 210 by the arms disrupt the vortices, leading to annihilation. The normalized circulation ($\tilde{\Gamma}$) 211 compares both 212 *Microvelia* and the physical model, revealing that optimal inter-stroke intervals 213 enhance re-energization

214 and thrust (Figures S4, S5). Vortical re-energization 215 in *Microvelia* doesn't always imply $\tilde{\Gamma} > 1$ due to reduced 216 hind legs' tarsal speed, imparting less energy 217 to the vortices (Figure 2.e).

218 **CFD analysis of thrust enhancement during vortex re-energization.** We simulate thrust 219 enhancement 220 through vortex capture using 2D CFD 221 models of high aspect ratio ($AR = 20$) 222 rectangular 223 plates undergoing prescribed rotation and translation. Mimicking the physical model configuration, 224 the first plate rotates counterclockwise, and the second plate rotates clockwise, starting with a time gap (Δt), 225 traversing the first plate's vortical wake (SI Video 227 4, Figure S5). These simulations evaluate the role of 228 vortex re-energization on thrust via robotic arms' trajectory rather than mimicking the precise kinematics 229 of 230 *Microvelia*.

231 Streamline analysis shows differences in flow velocity magnitudes for different Δt intervals (Figure 233 4.e). For 232 $\Delta t = 0.2$ s, the second plate captures

234 the first plate's wake, entering its recirculation region 235 closely (SI video 4). As a result, the vortex cores with 236 the same sense of rotation from both plates co-align 237 to increase the resultant circulation, augmenting the 238 propulsive force. In contrast, for $\Delta t = 0.5$ s, the sec-

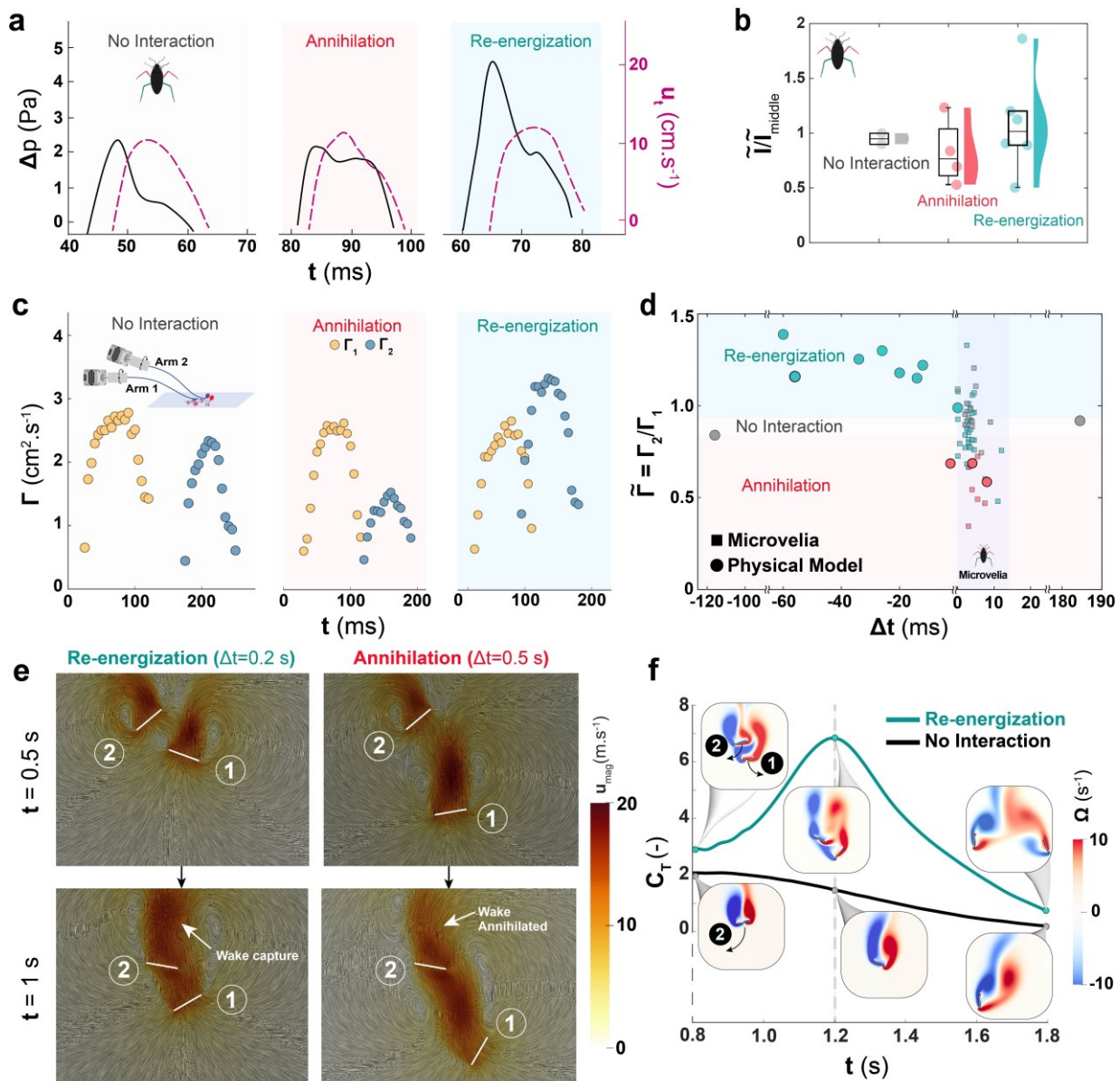


Figure 4: Quantifying epineuston vortical interactions through physical models and CFD analysis. **(a)** Temporal evolution of relative pressure (ΔP) and tarsal speed (v_t) of the hind leg. No-interaction and annihilation cases represent the hind left tarsi, while re-energization corresponds to the hind right tarsi. **(b)** Normalized impulse for different types of vortical interaction. The semi-violin plot shows the distribution of the data as a jitter plot, while the box and whisker plot represent the median and the four quartiles (25%, 50%, 75%, and 100%) for *Microvelia* specimens ($N=3$) and strokes ($n=12$). **(c)** Temporal evolution of the vortex circulation Γ for each robotic arm with varying Δt showing different vortical interaction outcomes. **(d)** Regime map of normalized circulation (Γ_2/Γ_1) for varying Δt . Γ_1 and Γ_2 represent peak circulation from the middle leg (or first arm) and hind leg (or second arm), respectively ($N=7$, $n=53$). **(e)** CFD results showing effect of the time interval between plate movements (in quiescent fluid) on vortical interactions depicted by velocity magnitude contours. The second plate starts moving at $t = 0$ s with $\Delta t = 0.2$ s for re-energization and $\Delta t = 0.5$ s for annihilation. In snapshots at $t = 1$ s, arrows indicate the enhanced and reduced velocity field due to wake capture and wake annihilation respectively. **(f)** Temporal evolution of the coefficient of thrust (C_T) of the second plate for re-energization and no interaction. Snapshots show the interaction's impact on instantaneous vorticity fields at different times.

291 and positioning of leg strokes enhance thrust through 292 vortex re-energization, offering new insights into fluid 293 dynamics at the air-water interface. Exploring mi₂₉₄ crovelia juvenile nymphs, multiphase CFD simulations, and turbulent flow regimes will further deepen 296 our understanding of these interactions.

297 By uncovering the physics behind the vortical re₂₉₈ capture in *Microvelia*, we extend similar mechanisms 299 observed in jellyfish and fruit flies to the neuston [5, 300 11, 301 12]. Epineuston vortex recapture could inspire 301 the development of efficient water-skating devices and 302 amphibious robots, enhancing our exploration of the 303 oceanic and freshwater neuston niches [26].

304 ACKNOWLEDGMENTS

305 The authors thank the members of the Bhamla Lab 306 for their feedback and useful discussions. MSB ac₃₀₇ knowledges funding support from the NSF Grants 308 CAREER 1941933 and PHY-2310691, and gift fund₃₀₉ ing from the Open Philanthropy Project. PR ac₃₁₀ knowledges the funding support from the Eckert 311 Postdoctoral Fellowship, Georgia Tech. J.O. ac₃₁₂ knowledges funding support from the GT UCEM fel₃₁₃ lowship program and the Herbert P. Haley fellowship 314 program.

315 COMPETING INTERESTS

316 The authors declare no competing 317 interests.

REFERENCES

318 [1] John O Dabiri. Optimal vortex formation as a 319 unifying principle in biological propulsion. *Annual review of fluid mechanics*, 41:17–33, 2009.

321 [2] PF Linden and JS Turner. ‘Optimal’ vortex rings 322 and aquatic propulsion mechanisms. *Proceedings 323 of the Royal Society of London. Series B: Biological Sciences*, 271(1539):647–653, 2004.

325 [3] Erik J Anderson and M Edwin DeMont. The me₃₂₆chanics of locomotion in the squid *loligo pealei*: 327 locomotory function and unsteady hydrodynamics of the jet and intramantle pressure. *Journal of Experimental Biology*, 203(18):2851–2863, 2000.

331 [4] Michael S Triantafyllou, GS Triantafyllou, and 332 DKP Yue. Hydrodynamics of fishlike swimming. 333 *Annual review of fluid mechanics*, 32(1):33–53, 2000.

335 [5] John H Costello, Sean P Colin, John O Dabiri, 336 Brad J Gemmell, Kelsey N Lucas, and Kelly R

Sutherland. The hydrodynamics of jellyfish 337 swimming. *Annual Review of Marine Science*, 338 13:375–396, 2021.

[6] Iztok Lebar Bajec and Frank H Heppner. Organized flight in birds. *Animal Behaviour*, 78(4):777–789, 2009.

[7] John Roger Speakman and D Banks. The function of flight formations in greylag geese *anser anser*; energy saving or orientation? *International Journal of Avian Science*, 140(2):280–287, 1998.

[8] Hao Liu, Shizhao Wang, and Tianshu Liu. Vortices and forces in biological flight: Insects, birds, and bats. *Annual Review of Fluid Mechanics*, 56:147–170, 2024.

[9] You-Jun Lin, Sheng-Kai Chang, Yu-Hsiang Lai, and Jing-Tang Yang. Beneficial wake-capture effect for forward propulsion with a restrained wing-pitch motion of a butterfly. *Royal Society open science*, 8(8):202172, 2021.

[10] Nils B Tack, Kevin T Du Clos, and Brad J Gemmell. Fish can use coordinated fin motions to recapture their own vortex wake energy. *Royal Society Open Science*, 11(1):231265, 2024.

[11] Brad J Gemmell, Sean P Colin, and John H Costello. Widespread utilization of passive energy recapture in swimming medusae. *Journal of Experimental Biology*, 221(1):jeb168575, 2018.

[12] Fritz-Olaf Lehmann, Hao Wang, and Thomas Engels. Vortex trapping recaptures energy in flying fruit flies. *Scientific Reports*, 11(1):6992, 2021.

[13] Michael H Dickinson, Fritz-Olaf Lehmann, and Sanjay P Sane. Wing rotation and the aerodynamic basis of insect flight. *Science*, 284(5422):1954–1960, 1999.

[14] David N Beal, Franz S Hover, Michael S Triantafyllou, James C Liao, and George V Lauder. Passive propulsion in vortex wakes. *Journal of fluid mechanics*, 549:385–402, 2006.

[15] Liang Li, M’at’e Nagy, Jacob M Graving, Joseph Bak-Coleman, Guangming Xie, and Iain D Couzin. Vortex phase matching as a strategy

422 namics of water-walking arthropods. *Journal of* 470
423 *Fluid Mechanics*, 644:5–33, 2010. pha). *Systematic Zoology*, 28(4):554–578, 1979. 471

424 [25] Zexiang Huang, Hao Yang, Ke Xu, Jianing Wu, [35] Miguel Pin˜eirua, Anna Verbe, and J’er^ome 472 425 and Jinxiu
425 Zhang. Collecting differently sized Casas. Substrate-mediated leg interactions play 473 426 particles on water
426 surface by maneuvering pedal a key role in insect stability on granular slopes. 474
427 waves on the foot of the water snail pomacea 475
428 canaliculata. *Soft Matter*, 18(40):7850–7858, 2023.

429 [36] Antoine Humeau, Miguel Pin˜eirua, J’er^ome Cras- 476
430 2022. 476 sous, and J’er^ome Casas. Locomotion of ants 477 430
431 mysterious ecosys- walking up slippery slopes of granular materi- 478 431
432 PLoS Biology, 19(4):e3001046, 2021. 480 481 [37] Pavan Ramdy, Robin Thandiackal, Raphael [47] Stephen P Yanoviak
433 and DN Frederick. Water 527 482 Cherney, Thibault Asselborn, Richard Benton, surface locomotion in tropical canopy ants.
434 Jour- 528 483 Auke Jan Ijspeert, and Dario Floreano. Climb- 529
435 ing favours the tripod gait over alternative faster 2014. 530
436 insect gaits. *Nature communications*, 8(1):14494,
437 2017.

438 [38] Lanna Cheng. 488 Marine and freshwater skaters: 488 differences in surface fine structures. 489
439 242(5393):132–133, 1973. 489 *Nature*,
490 [39] Nils Møller Andersen. Fine structure of the body 491
491 hair layers and morphology of the spiracles of 492
492 semiaquatic bugs (insecta, hemiptera, gerromor- 493 pha) in
493 relation to life on the water surface. *Vi494dansk. Medd. Dansk*
494 *Naturhist. Foren.*, 140:7–37,
495 1977.

496 [40] C’edric Finet, Am’elie Decaras, Maria 497 Rutkowska, Pascale Roux,
497 Samuel Collaudin, 498 Pauline Joncour, S’everine Viala, and Abder 499
498 rahman Khila. Leg length and bristle density, 500 both necessary for
499 water surface locomotion, 501 are genetically correlated in water striders.
500 *Proceedings of the National Academy of Sciences*, 503
501 119(9):e2119210119, 2022.

502 [41] ABD Cassie and S Baxter. Wettability of porous
503 surfaces. 504 *Transactions of the Faraday society*, 506 40:546–551, 1944.

505 [42] William Gilpin, Vivek N Prakash, and Manu 508
506 Prakash. Flowtrace: simple visualization of co509 herent
507 structures in biological fluid flows. *Jour510 nal of*
508 *experimental biology*, 220(19):3411–3418,
509 2017.

510 [43] William Thielicke and Ren’e Sonntag. Particle 513 image velocimetry for
511 matlab: Accuracy and en514 hanced algorithms in pivlab. *Journal of Open* 515
512 *Research Software*, 9(1), 2021.

⁵¹⁶ [44] Michael Krieg and Kamran Mohseni. Modelling ⁵¹⁷ circulation, impulse and kinetic energy of start⁵¹⁸ ing jets with non-zero radial velocity. *Journal of* ⁵¹⁹ *Fluid Mechanics*, 719:488–526, 2013.

⁵²⁰ [45] Robert B Suter. Spider locomotion on the water ⁵²¹ surface: biomechanics and diversity. *The Jour*⁵²² *nal of Arachnology*, 41(2):93–101, 2013.

⁵²³ [46] Thomas Steinmann, Antoine Cribellier, and ⁵²⁴ Jérôme Casas. Singularity of the water strider ⁵²⁵ propulsion mechanisms. *Journal of Fluid Me*⁵²⁶ *chanics*, 915, 2021.